Journal of Materials Chemistry A

PAPER

View Article Online
View Journal

Cite this: DOI: 10.1039/c7ta11138j

Development of a photo-catalytic converter for potential use in the detoxification of Cr(VI) metal in water from natural resources

Prasenjit Kar,[a] Tuhin Kumar Maji,[a] Probir Kumar Sarkar,[ab] Peter Lemmens[cd] and Samir Kumar Pal *[a]

Porphyrin dye sensitized nanomaterials (nanohybrids) are advantageous for application in photocatalysis due to their additional absorption band that matches the solar irradiance spectrum. Here we have impregnated protoporphyrin IX with copper(II) ions and sensitized porous TiO_2 microspheres (~1.5 μm in diameter) in order to synthesize a functional nanohybrid for application in visible light photocatalysis. While electron microscopy studies (FESEM and HRTEM) confirm the inorganic porous structure of the microspheres, Fourier transform infrared (FTIR), electronic spectroscopy and picosecond resolved fluorescence studies on the sensitizing PP molecules reveal the formation of the functional nanohybrid. Hexavalent chromium (Cr(VI)) in the aquatic environment is a commonly identified proven carcinogenic heavy metal pollutant, whereas Cr(III) is nontoxic and considered to be an essential nutrient for living organisms. We have applied the nanohybrid for an efficient reduction of toxic Cr(VI) metal ions to non-toxic Cr(III) in water under visible light illumination. The advantage of the Cu ion impregnation into the sensitizing PP dye is evident from the intact efficacy in the photocatalytic reduction in the presence of water dissolved metal ions (Cr^{3+} and Fe^{3+}) is confirmed from our study. On the other hand, the nanohybrid without the Cu(II) suffers from interference from other dissolved metal ions during the photocatalytic reduction process. For a prototype application, we have developed an active filter (having physical and chemical filtering capability) by depositing the nanohybrid on an extended surface of a stainless-steel metal mesh (size 2 cm × 2 cm, pore size 150 μm × 200 μm). The prototype active filter exhibits significant potential for chemical filtering of toxic Cr(VI) ions (photoreduction to Cr(III)) along with physical cleaning of suspended particulates present in water.

Received 21st December 2017
Accepted 25th January 2018

DOI: 10.1039/c7ta11138j

rsc.li/materials-a

1. Introduction

Nanohybrids are a class of newly developed hybrid materials consisting of organic/inorganic dyes and inorganic nanoparticles, and have been extensively used in photocatalysis.[1–3] Furthermore, nanohybrids are characterized by tailorable chemistry with improved charge separation and light absorption ability. Therefore, the development of low cost and highly efficient nanohybrids is very much essential, and it relies on the suitable choice of dyes used in light harvesting. In this context, the use of ruthenium-based inorganic dyes is inefficient for photocatalytic application as it is very expensive.[4] Moreover, the toxicity and possible incomplete mineralization of ruthenium-based inorganic dyes will pose a risk of secondary contamination during the photocatalytic process.[5,6] In contrast, the use of porphyrin from natural resources is very efficient in light harvesting for practical photocatalytic application as it is both cost effective and less toxic as compared to ruthenium based inorganic dyes. Our previous studies on hematoporphyrin sensitized ZnO nanorods indicated dual applications in efficient visible-light photocatalysis (VLP) and dye-sensitized solar cells (DSSC).[7] Afzal *et al.* have demonstrated that meso-tetra(4-carboxyphenyl) porphyrin (TCPP)-sensitized TiO_2 exhibits superior self-cleaning properties for degradation of methylene blue under visible-light illumination.[8]

Hexavalent chromium contamination in drinking water is one of the most severe problems resulting from discharge of industrial effluents.[9–13] Highly water soluble hexavalent chromium has been proved to be a human carcinogen because it readily penetrates cell membranes to produce several unstable intermediates and reactive oxygen species (ROS).[14–16] In addition, hexavalent chromium intermediates and ROS cause damage to DNA and mutagenesis.[17] Thus, reduction of Cr(VI) to

[a]Department of Chemical, Biological and Macromolecular Sciences, S. N. Bose National Centre for Basic Sciences, Block JD, Sector III, Salt Lake, Kolkata 700 106, India. E-mail: skpal@bose.res.in

[b]Department of Physics, Ananda Mohan College, 102/1, Raja Rammohan Sarani, Kolkata–700009, India

[c]Institute for Condensed Matter Physics, TU Braunschweig, Mendelssohnstraße 3, 38106 Braunschweig, Germany

[d]Laboratory for Emerging Nanometrology, TU Braunschweig, Braunschweig, Germany

Cr(III) is very much beneficial because Cr(III) does not pose any toxicological hazard. For the removal of toxic pollutants from the environment, photocatalysis technology is a highly appealing green approach for practical application compared to other commonly used techniques, such as adsorption, chemical reduction, electrochemical methods, bioremediation, and ion exchange.[18–25] In recent studies employing several nanomaterials,[26,27] attempts have been made to reduce toxic Cr(VI) to nontoxic Cr(III).[28–30] Utilizing visible light photocatalytic techniques using several nano-composites for the above-mentioned reduction has also been reported in the literature.[31–34] It has to be noted that mere reduction of the toxic Cr(VI) to Cr(III) may not be sufficient for the complete detoxification of water from chromium hazards for the following reasons. While chromium(VI) oxide is an example of an excellent water-soluble chromium compound (solubility = 1680 g L^{-1}), the reduced product, chromium(III), is water insoluble and may be deposited on the surface of the nanocatalysts, affecting their long-term stability. The reduced product, chromium(III), can also be bound to floating suspended particulates in water. Given the possibility of re-oxidation of Cr(III) to Cr(VI) under various conditions pertaining to the natural environment,[35] complete removal of suspended particulates from the treated water is essential for complete chromium detoxification. The recyclability of the catalyst, which plays an important role in its repetitive reduction capability, is also an important requirement which has been rarely addressed in the literature.[29]

In the present work, we have successfully synthesized (Cu)PP–TiO_2 nanohybrids where copper metalated protoporphyrin is covalently attached to porous TiO_2 microspheres ((Cu)PP–TiO_2). We observed excellent photocatalytic activity of the (Cu)PP–TiO_2 nanohybrid for the reduction of toxic metal Cr(VI) under visible light illumination. A detailed electron microscopy and optical spectroscopy characterization of the synthesized nanohybrid has also been performed. The recyclability of the (Cu)PP–TiO_2 nanohybrid for the repetitive reduction of the toxic Cr(VI) ions even in the presence of interfering Cr(III) and Fe(III) is confirmed, revealing long term stability of the material for its practical use. In order to fabricate a prototype device, which would not only reduce the soluble Cr(VI) ions, but also physically filter suspended particulates containing reduced Cr(III), we have deposited the (Cu)PP–TiO_2 nanohybrid on a stainless-steel metal mesh (size 2 cm × 2 cm, pore size 150 μm × 200 μm). In our opinion, the developed strategy would be beneficial for chromium detoxification in real world water samples.

2. Experimental section

2.1. Reagents

Protoporphyrin IX (PP), methylene blue (MB), ferric chloride ($FeCl_3$), chromium(III) chloride hexahydrate ($CrCl_3 \cdot 6H_2O$), copper(II) sulphate pentahydrate ($CuSO_4 \cdot 5H_2O$), titanium isopropoxide, and 1,5-diphenylcarbazide were purchased from Sigma-Aldrich. Potassium dichromate ($K_2Cr_2O_7$) and potassium persulfate ($K_2S_2O_8$) were purchased from Merck. Ultrapure water (Millipore System, 18.2 MΩ cm) and dimethyl sulfoxide (DMSO) (purchased from Merck) were used as solvents. All other chemicals used in the study were of analytical grade and were used without further purification.

2.2. Synthesis of TiO_2 microspheres

In a typical synthesis of TiO_2 microspheres, 1 mL of titanium isopropoxide was mixed with 15 mL of anhydrous acetone and then stirred for 15 min.[36,37] Then the solution was transferred into a 20 mL Teflon lined stainless-steel autoclave and heated at 180 °C for 12 h without shaking. The system was then cooled to ambient temperature naturally. The final product was collected and washed with acetone and absolute alcohol several times. Then the as-prepared samples were further annealed at 400 °C for 5 h in air in order to improve their crystallinity.

2.3. Sensitization of TiO_2 microspheres with PP, Fe(III)PP, Cr(III)PP and Cu(II)PP

A 0.5 mM PP ($C_{34}H_{36}N_4O_5$) solution was prepared in a mixture of dimethyl sulfoxide (DMSO) and deionized (DI) water (1 : 1, v/v) under constant stirring for 1 h. Sensitization of PP with TiO_2 microspheres was done by the addition of TiO_2 microspheres into PP followed by overnight stirring. Next, the nanohybrid was filtered out and washed several times with DMSO–water in order to remove unbound PP. Finally, the as-synthesized nanohybrid was dried in an oven and put in the dark until further use. The synthesis of Cr(III)PP, Fe(III)PP and Cu(II)PP was carried out by the addition of 1 : 1 PP (0.5 mM) and chromium chloride hexahydrate ($CrCl_3 \cdot 6H_2O$), ferric chloride ($FeCl_3$), or copper sulphate pentahydrate ($CuSO_4 \cdot 5H_2O$), followed by overnight stirring. Next, sensitization with TiO_2 microspheres was performed by a method similar to the one described above.

For the determination of the amount of PP dye loading in the nanohybrid, we have performed the two following experiments. Firstly, the PP in a measured amount of nanohybrid was washed out by using a solution mixture of 0.1 M sodium hydroxide and DMSO (1 : 1 vol%). The concentration of PP in the nanohybrid was measured by using UV-VIS spectroscopy, and we found that 3.6 wt% of PP was attached to the TiO_2 microspheres. Secondly, we examined the weight loss of the nanohybrid in thermogravimetric studies. We found a consistent result of 3.6 wt% of PP loading in the nanohybrid as obtained from the former investigation.

2.4. Fabrication of PP–TiO_2 and (Cu)PP–TiO_2 nanohybrids on a mesh

For the fabrication of nanohybrids on a stainless-steel mesh, initially the mesh was cleaned through bath sonication in acetone for 30 min and dried on a hot-plate at 60 °C. At first, the TiO_2 seed layer was deposited on the cleaned mesh using a nebulizer, which was followed by annealing at 400 °C for 5 h. This layer was used as a seeding layer for the synthesis of TiO_2 microspheres. Then the TiO_2 seeded mesh was immersed in a 20 mL Teflon-lined stainless-steel autoclave containing titanium isopropoxide solution. The Teflon-lined autoclave was put into an oven at 180 °C for 12 h. The system was then cooled to ambient temperature naturally. The mesh was collected and

washed several times with acetone followed by ethanol. Then the mesh was annealed at 400 °C for 5 h. Next, sensitization of the TiO_2 microsphere embedded mesh was performed by overnight stirring with 0.5 mM PP and (Cu)PP. Finally, the nanohybrid embedded mesh was washed several times with DMSO–water in order to remove unbound PP.

2.5. Characterization methods

A field emission scanning electron microscopy (FESEM, QUANTAFEG 250) investigation was performed by applying a diluted drop of TiO_2 microspheres on a silicon wafer. Transmission electron microscopy (TEM) grids of TiO_2 microspheres were prepared by applying a diluted drop of the sample to carbon-coated copper grids. The particle sizes were determined from micrographs recorded at a magnification of 100 000× using an FEI (Technai S-Twin, operating at 200 kV) instrument. X-ray diffraction (XRD) patterns of the TiO_2 microspheres were recorded by employing a scan rate of 0.02° s^{-1} in the 2θ range from 20° to 80° using a PANalytical XPERTPRO diffractometer equipped with Cu Kα radiation (at 40 mA and 40 kV). For optical experiments, steady-state absorption and emission measurements were carried out with a Shimadzu UV-2600 spectrophotometer and a Jobin Yvon Fluoromax-3 fluorimeter, respectively. FTIR spectra were recorded on a JASCO FTIR-6300 spectrometer, using a CaF_2 window. For steady state and time resolved optical studies, we have followed the methodology described in our earlier work.[38]

2.6. Photocatalytic performance measurements

The photocatalytic activity of the samples was evaluated by photocatalytic reduction of Cr(VI) at ambient temperature. The photodegradation reaction of Cr(VI) was carried out in a reactor containing $K_2Cr_2O_7$ aqueous solution (20 mg L^{-1}) as a test contaminant along with the photocatalyst (1 g L^{-1}). The suspension was irradiated with a mercury lamp (under visible light, $\lambda \geq 400$ nm) and absorbance data were collected continuously by UV-Vis spectroscopy. The Cr(VI) reduction was determined colorimetrically at 540 nm using a 1,5-diphenylcarbazide (DPC) colorimetric method.[12,39] The percentage degradation (% DE) of Cr(VI) was determined using the equation

$$\%\ \mathrm{DE} = \frac{I_0 - I}{I_0} \times 100 \quad (1)$$

where I_0 is the initial absorption intensity of the Cr–DPC complex at $\lambda_{max} = 540$ nm and I is the absorption intensity after irradiation.

3. Results and discussion

Fig. 1a shows the XRD pattern of the as-synthesized TiO_2 microspheres after annealing at 400 °C. All the diffraction peaks are consistent with the tetragonal anatase phase.[40] Fig. 1b shows an FESEM image of TiO_2 microspheres with an average diameter of 1–1.5 μm. The TiO_2 microspheres are perfectly spherical and composed of interconnected nanocrystals as revealed in Fig. 1c. The HRTEM image of a TiO_2 microsphere

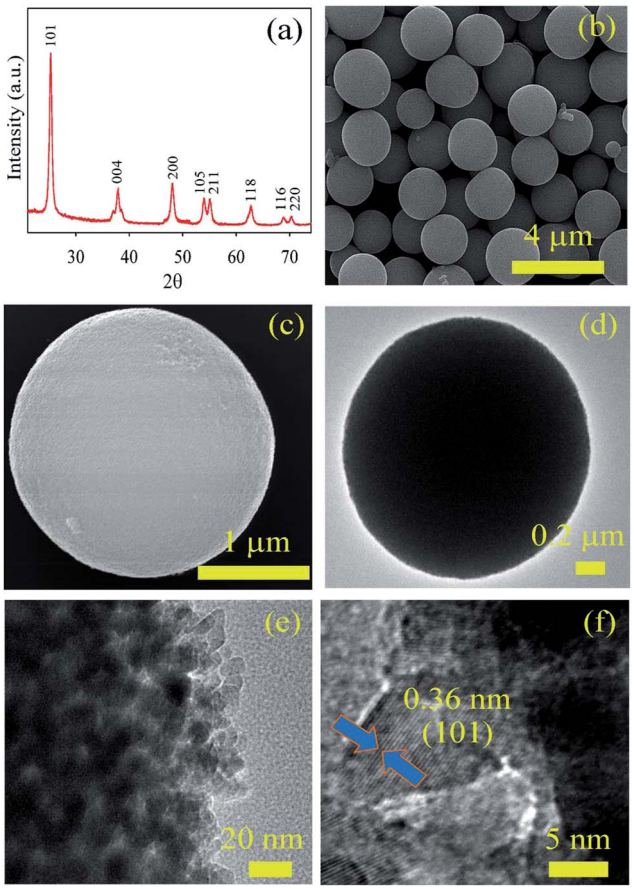

Fig. 1 (a) XRD pattern of TiO_2 microspheres. (b and c) FESEM images of TiO_2 microspheres. (d) TEM and (e and f) HRTEM images of TiO_2 microspheres.

(Fig. 1d) further demonstrates pores (10–12 nm) in the boundary of two interconnected nanoparticles in the microsphere (Fig. 1e and f). Furthermore, the HRTEM analysis in Fig. 1f shows lattice fringes with an interlayer distance of 0.36 nm, which is close to the 0.352 nm lattice spacing of the (101) planes in anatase TiO_2, which is consistent with XRD results (Fig. 1a).

In order to evaluate interaction between PP and TiO_2 microspheres present in the nanohybrid, we have performed Fourier-transform infrared (FTIR) spectroscopic studies. From Fig. 2a it is clear that free PP shows two characteristic antisymmetric and symmetric stretching vibrations for the carboxylic group, located at 1698 and 1402 cm^{-1} respectively. Therefore, the difference in the stretching frequency ($\Delta = \gamma_{as} - \gamma_{sym}$) of the carboxylic group is indicative of the binding of PP upon attachment on the nanoparticle surface.[41] After binding with TiO_2 microspheres, the stretching frequency of the carboxylic group is shifted to 1634 and 1403 cm^{-1} for the antisymmetric and symmetric stretching vibrations respectively. The observed Δ value for PP–TiO_2 (231 cm^{-1}) is lower compared to that of the free PP (296 cm^{-1}), indicating bidentate covalent binding of PP on the host TiO_2 surface.[38] The incorporation of metal ions into the porphyrin moiety has been confirmed from the perturbation of the N–H stretching frequency as revealed by the FTIR experiment (Fig. 2b).

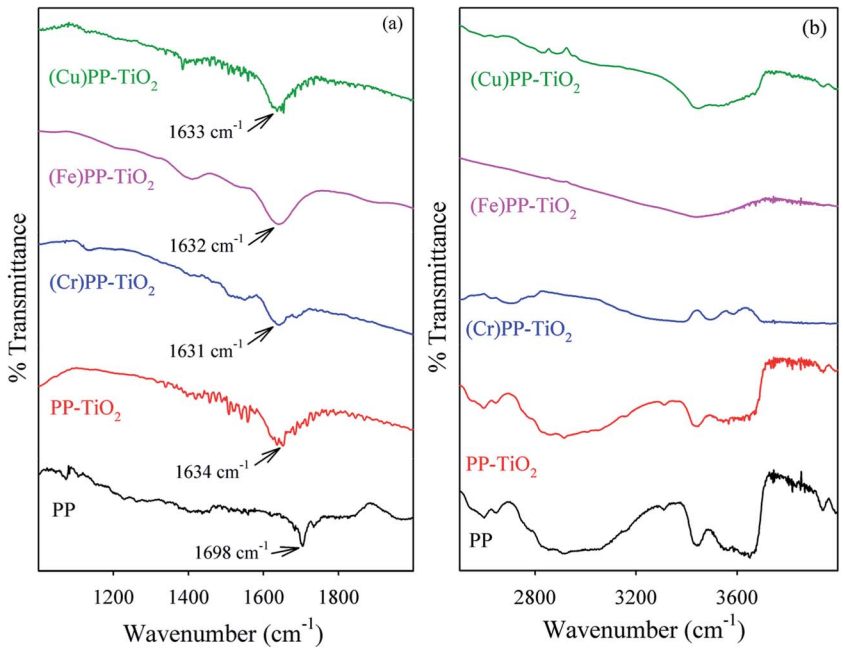

Fig. 2 (a) FTIR spectra of PP, PP–TiO_2, (Cr)PP–TiO_2, (Fe)PP–TiO_2 and (Cu)PP–TiO_2. (b) FTIR spectra of PP, PP–TiO_2, (Cr)PP–TiO_2, (Fe)PP–TiO_2 and (Cu)PP–TiO_2.

For free PP, the N–H stretching frequency is found to be at 3441 cm^{-1}, as shown in Fig. 2b. In PP–TiO_2, the N–H stretching frequency remains unperturbed, indicating that PP anchors on TiO_2 through the carboxylic functional group only. However, perturbation of the N–H stretching frequency is observed in the presence of metal ions (Cu^{2+}, Fe^{3+} and Cr^{3+}), confirming the successful binding of the metal ions to the PP through the central pyrrole nitrogen atoms.

Fig. 3a shows the absorption spectrum of the synthesized PP–TiO_2 nanohybrid. A reference PP sensitizer is also shown for comparison. PP having extensively delocalized π electrons exhibits a Soret band at 409 nm along with Q bands between 500 and 700 nm.[42,43] The formation of J and H types of aggregates for PP in DMSO–water is evident from the spectra.[44,45] After attachment of PP on the TiO_2 surface, the Soret band is red-shifted along with disappearance of aggregation, indicating interaction between carboxylic groups of PP and TiO_2.[38,46] Similar results were observed for other metalated nanohybrids (data not shown). Fig. 3b shows the fluorescence spectra of PP upon excitation at the Soret band. However, after metalation, the emission intensity of PP is significantly decreased indicating excited state charge transfer transitions responsible for fluorescence quenching.[7,47]

The photocatalytic activity of the as-synthesized nanohybrids is investigated by visible light reduction of Cr(VI) in aqueous solution at room temperature. Fig. 4a shows the time dependent UV-Vis absorption spectra of the DPC–Cr(VI) complex solution peaking at 540 nm under visible light illumination in the presence of (Cu)PP–TiO_2. Fig. 4b shows the photocatalytic reduction of Cr(VI) as indicated by the decreased optical density at 540 nm as a function of irradiation time using different photocatalysts. Prior to illumination, the solution was

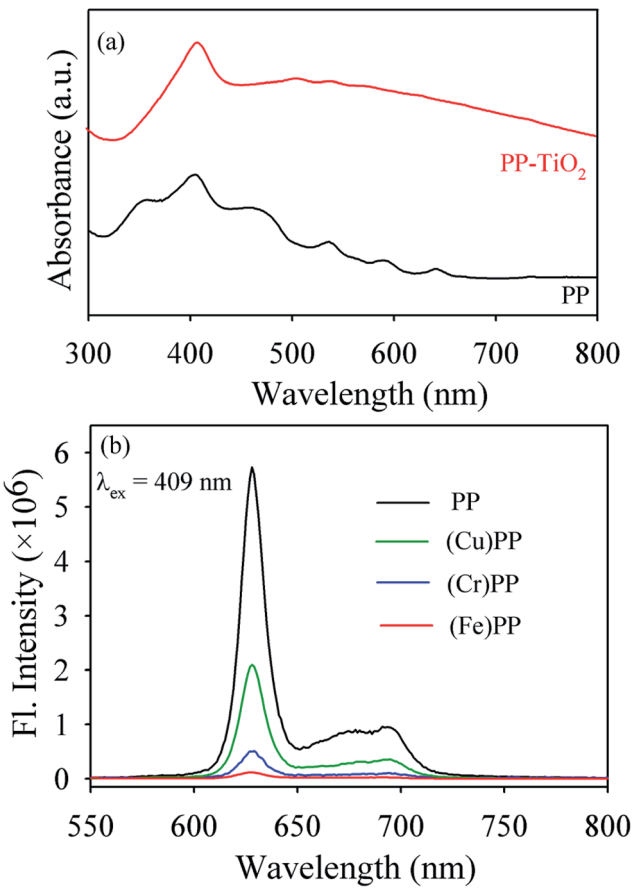

Fig. 3 (a) UV-Vis absorption spectra of PP and PP–TiO_2. (b) Room temperature fluorescence spectra of PP, (Cu)PP, (Cr)PP and (Fe)PP.

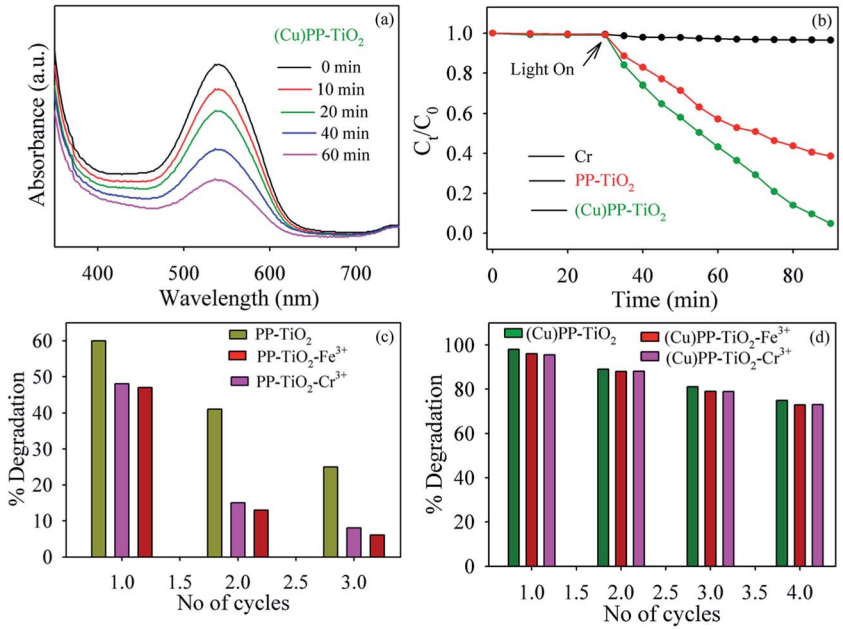

Fig. 4 (a) UV-Vis absorption spectra for the photocatalytic reduction of Cr(VI) by (Cu)PP–TiO_2 under visible light. (b) Photocatalytic reduction of Cr(VI) under visible light in the presence and absence of nanohybrids. (c) Recyclability study of PP–TiO_2 in the presence of $Fe^{3+}$and Cr^{3+} ions for the reduction of Cr(VI). (d) Recyclability study of (Cu)PP–TiO_2 in the presence of Fe^{3+} and Cr^{3+} ions for the reduction of Cr(VI).

magnetically stirred for 30 minutes in the dark to achieve adsorption equilibrium of the toxic Cr(VI) on the nanohybrids. With our experimental time window, photocatalytic reduction of Cr(VI) in the absence of photocatalysts was almost negligible. In contrast, PP–TiO_2 nanohybrids show enhanced photocatalytic activity and 60% photoreduction of Cr(VI) is observed after 60 minutes of visible light illumination. Upon incorporation of copper(II) metal ions into the porphyrin moiety, (Cu)PP–TiO_2 nanohybrids further enhance the photocatalytic activity (~100%) compared to PP–TiO_2 (60%). A brief review of contemporary literature reveals that in comparison with other reported catalysts for the reduction of Cr(VI), our nanohybrids, *i.e.* (Cu)PP–TiO_2 nanohybrids, exhibit better photocatalytic performance.[48–52] From the application point of view, the stability of the photocatalysts is also an important parameter for evaluating their performance as it could reduce the cost of the

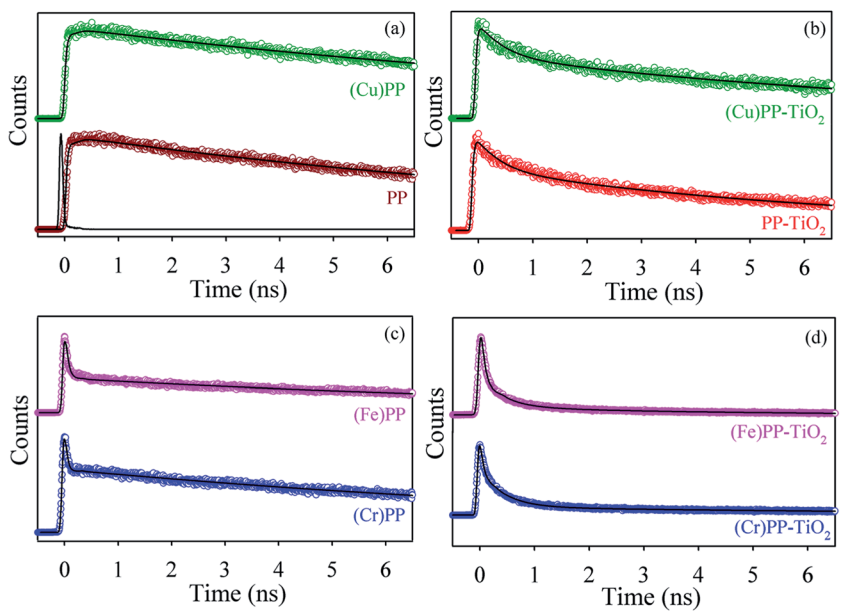

Fig. 5 Fluorescence decay profiles of (a) PP (violet) and (Cu)PP (dark green), (b) PP–TiO_2 (red) and (Cu)PP–TiO_2 (dark green), (c) (Cr)PP (blue) and (Fe)PP (pink), and (d) (Cr)PP–TiO_2 (blue) and (Fe)PP–TiO_2 (pink) detected at 630 nm upon excitation at a wavelength of 409 nm.

Table 1 Lifetimes of picosecond time-resolved fluorescence transients of different samples detected at 630 nm PL maxima upon excitation at 409 nm wavelength. The values in parentheses represent the relative weight percentages of the time components

System	τ_1 (ps)	τ_2 (ps)	τ_3 (ps)	τ_{avg} (ns)
PP	12 200 (100%)			12.2
(Cu)PP	12 100 (100%)			12.1
(Cr)PP	39 (70%)	12 100 (30%)		3.65
(Fe)PP	50 (68%)	12 100 (32%)		3.9
PP–TiO_2	420 (39%)	7245 (61%)		4.53
(Cu)PP–TiO_2	420 (39%)	8519 (61%)		5.36
(Cr)PP–TiO_2	45 (67%)	414 (28%)	8583 (9%)	0.77
(Fe)PP–TiO_2	50 (72%)	370 (24%)	7865 (4%)	0.43

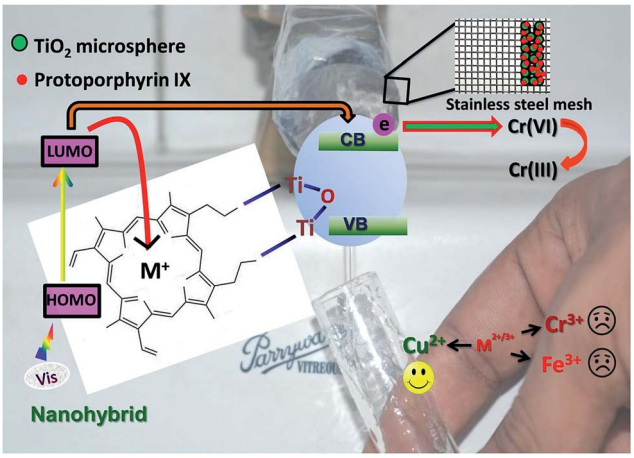

Scheme 1 Schematic representation of the photocatalytic reduction of Cr(VI) by the (Cu)PP–TiO_2 nanohybrid in the presence of water dissolved metal ions (Fe^{3+} and Cr^{3+}) under visible-light illumination.

respective process.[53,54] To confirm the stability of the photocatalytic nanohybrids, we further performed a recyclability study of (Cu)PP–TiO_2 and PP–TiO_2 nanohybrids in the presence and absence of water dissolved Fe^{3+} (0.07 mM) and Cr^{3+} (0.07 mM) ions. The metal ion concentration used in this study is above the WHO prescribed limit in ground water. In this context, the recyclability of the PP–TiO_2 nanohybrid decreases after each cycle and the loss is much more in the presence of dissolved metal ions as evident from Fig. 4c. From Fig. 4d it is evident that the (Cu)PP–TiO_2 nanohybrids exhibit excellent recyclability up to four cycles. Even in the presence of dissolved metal ions recyclability of (Cu)PP–TiO_2 is unaltered. Therefore, the reusability results predict the superiority of (Cu)PP–TiO_2 as a catalyst and support for promising use in waste water treatment.

In order to investigate the key ultrafast dynamical events which can modulate the photocatalytic activity of PP–TiO_2 in the presence of dissolved metal ions, we have performed picosecond-resolved fluorescence spectroscopy as shown in Fig. 5. The associated time constants are tabulated in Table 1. The observed faster component for (Fe)PP and (Cr)PP reveals excited state electron transfer from PP to metal ions (Fe^{3+} and Cr^{3+}). Our control experiment with PP shows a similar time component to that of (Cu)PP. This eventually rules out the excited state electron transfer from PP to Cu^{2+}. As shown in

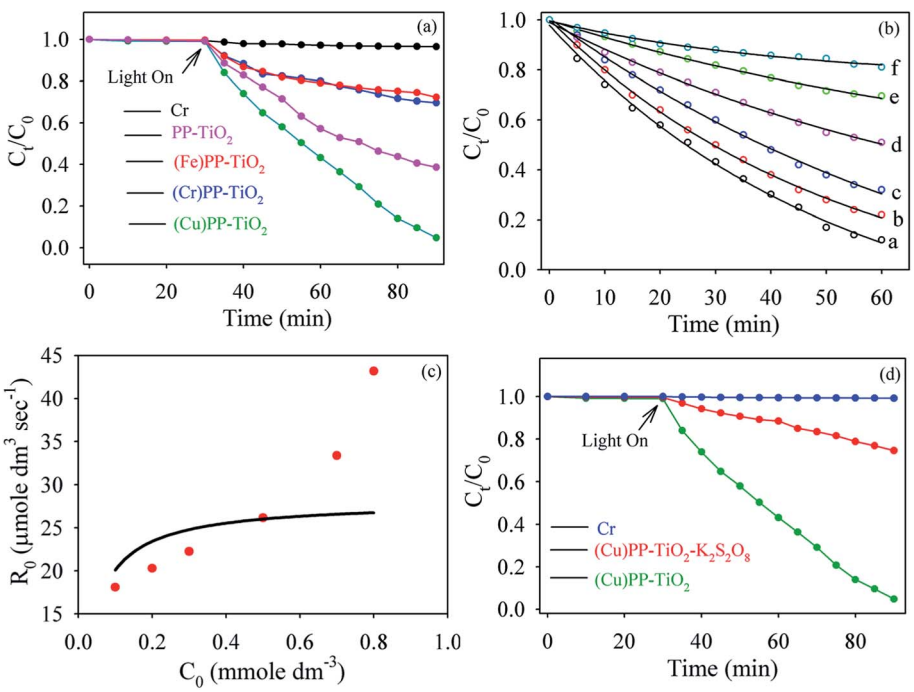

Fig. 6 (a) Photocatalytic reduction of Cr(VI) under visible light in the presence and absence of nanohybrids. (b) C_t/C_0 *versus* time with different concentrations of Cr(VI) during photocatalytic reduction using (Cu)PP–TiO_2 under visible light. (c) Langmuir–Hinshelwood (L–H) plot for photocatalytic reduction of Cr(VI) using (Cu)PP–TiO_2 (where the solid line is the model fitting and the solid circles represent experimental data). (d) Photocatalytic reduction of Cr(VI) by (Cu)PP–TiO_2 in the presence of $K_2S_2O_8$.

Fig. 5, the faster time component in the case of PP–TiO_2 may be attributed to the excited state electron transfer from PP to the host TiO_2 matrix. However, the fluorescence transient of (Cu) PP–TiO_2 is essentially comparable with that of PP–TiO_2. It has to be noted that in the presence of metal ions (Cr^{3+} and Fe^{3+}), fluorescence transients of PP–TiO_2 are eventually faster compared to those of PP–TiO_2. Thus, our observation demonstrated that additional electron migration pathways from PP to Cr^{3+}/Fe^{3+}ions modulate the photocatalytic activity of PP–TiO_2, as they significantly reduce the availability of electrons in the conduction band of TiO_2.

To understand the modulation of photocatalytic activity in the presence of dissolved metal ions, we purposely incorporated metal ions (Fe^{3+} and Cu^{2+}) into the porphyrin moiety. The photocatalytic activity of the nanohybrids was studied under visible light illumination as illustrated in Fig. 6a. Direct visible-light illumination without any catalyst can lead to insignificant reduction of Cr(VI). A photodegradation efficiency of 60% is achieved using PP–TiO_2 alone, while in the presence of copper within the porphyrin moiety almost complete reduction occurs within the same experimental time window. The increased photocatalytic activity in the presence of Cu(II) metal ions within the porphyrin moiety correlated with additional structural stability of the (Cu)PP–TiO_2 nanohybrid against photobleaching. The structural stability eventually leads to the generation of more electrons, which is responsible for the enhancement in the photoreduction ability of Cr(VI). Such enhancement in photocatalytic activity due to the presence of copper metal within the porphyrin moiety is reported in several literature studies.[43,47,55] In addition, the photocatalytic activity of (Cr)PP–TiO_2 and (Fe)PP–TiO_2 is significantly reduced compared to that of both PP–TiO_2 and (Cu)PP–TiO_2. This decrease in

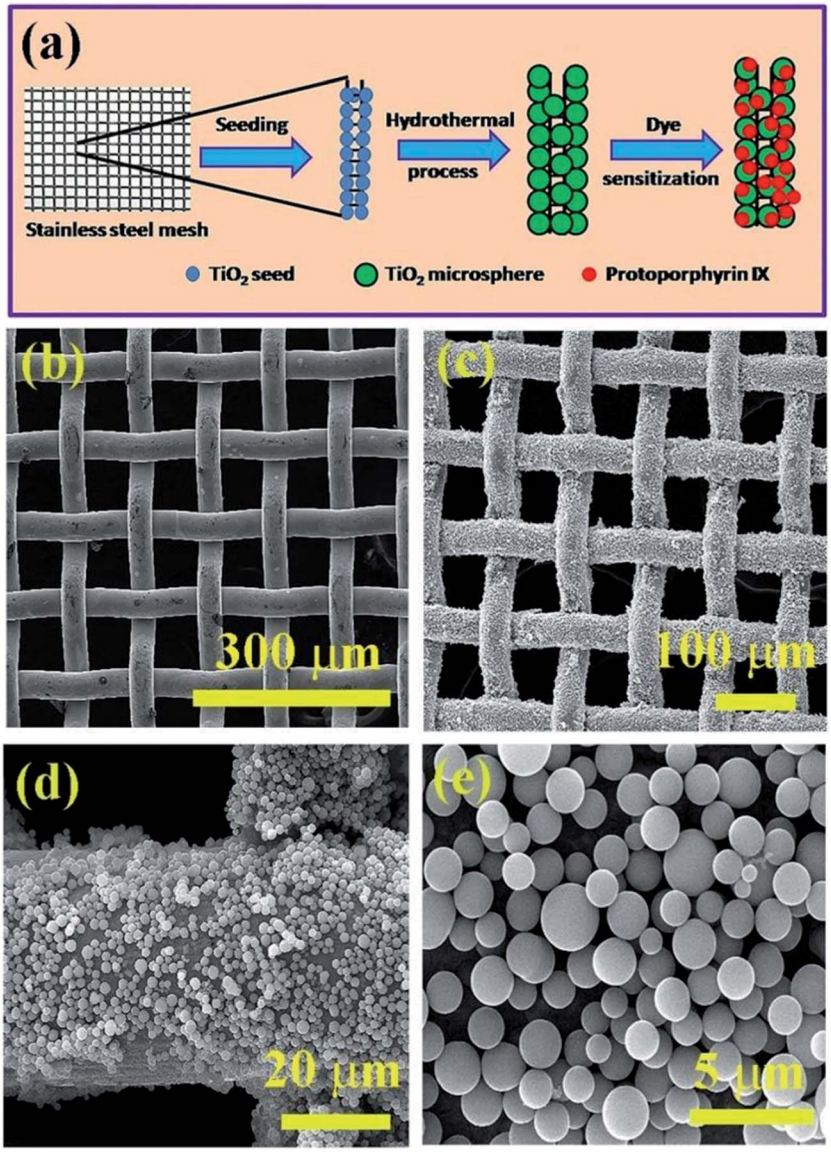

Fig. 7 (a) Schematic representation of TiO_2 microsphere synthesis on a stainless steel mesh. (b) SEM image of the bare stainless steel mesh. SEM images of TiO_2 on the mesh at low magnification (c and d) and high magnification (e).

photocatalytic activity in the presence of metals ions (Cr^{3+} and Cu^{2+}) is due to excited state electron transfer from PP to Cr^{3+}/Fe^{3+} and eventually reduced availability of electrons in the conduction band of TiO_2, as evident from a Time-Correlated Single Photon Counting (TCSPC) study. Our observation is also consistent with the result shown in Fig. 4c, where we use the metals ions as water contaminants for the recyclability study of PP–TiO_2. In order to find out the effect of the surface on photocatalysis, we further studied Langmuir–Hinshelwood (L–H) kinetics using different concentrations of Cr(VI) as shown in Fig. 6b. A significant deviation of the model (solid line) from experimental data (as shown in Fig. 6c) ruled out any role of the surface in the photodegradation of Cr(VI) under visible light illumination. To further illustrate the photocatalytic mechanism, we have used $K_2S_2O_8$ as a scavenger for photo-generated electrons.[56,57] Photoreduction of Cr(VI) under visible light illumination has been performed using the (Cu)PP–TiO_2 nanohybrid in the presence and absence of $K_2S_2O_8$. As shown in Fig. 6d, the presence of $K_2S_2O_8$ significantly inhibits the photocatalytic reduction of Cr(VI). The results demonstrate that photo-generated electrons in the nanohybrid indeed play a key role in the photocatalytic reduction of Cr(VI). On the basis of our experimental results and reported literature work,[33,57,58] the photocatalytic reduction reactions of Cr(VI) can be concluded to be distal rather than surface mediated L–H type and may be expressed by the following equations:

$$\text{(Cu)PP–TiO}_2 + \text{visible light} \rightarrow \text{(Cu)PP–TiO}_2\ (h + e) \quad (2)$$

$$Cr_2O_7^{2-} + 14H^+ + 6e \rightarrow 2Cr^{3+} + 7H_2O \quad (3)$$

$$2H_2O + 4h^+ \rightarrow O_2 + 4H^+ \quad (4)$$

Based on the above experiments, Scheme 1 provides a schematic representation of the photocatalytic reaction mechanism for the reduction of Cr(VI) using (Cu)PP–TiO_2.

In order to explore real world application, we have fabricated nanohybrids on a stainless-steel mesh for removal of toxic metal present in drinking water (Fig. 7a). The surface morphology of the stainless steel mesh and mesh coated TiO_2 microspheres was determined by FESEM. Fig. 7b–d show low magnification images of the bare mesh and TiO_2 microsphere coated mesh. The high magnification image of the TiO_2 microsphere coated mesh (Fig. 7e) shows uniform distribution of TiO_2 microspheres with diameters ranging from 1 to 1.5 μm. After decoration of TiO_2 microspheres on the mesh, we successfully sensitized the microspheres with PP and (Cu)PP. The photocatalytic reduction of Cr(VI) under visible light illumination has been studied using mesh embedded nanohybrids. From Fig. 8, it is evident that in the absence of light, the nanohybrids exhibit <2% surface adsorption. Furthermore, under solar light illumination, PP–TiO_2 exhibits 35% photocatalytic activity, while the incorporation of Cu metal into the porphyrin moiety increases the photocatalytic activity up to 50%. Under the same experimental conditions, Cr(VI) shows no photoreduction in the absence of the nanohybrids. From a practical application point of view,

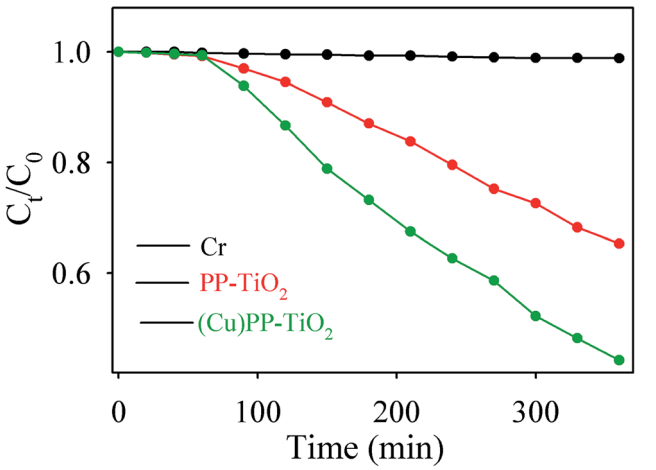

Fig. 8 Photocatalytic reduction of Cr(VI) by PP–TiO_2 and (Cu)PP–TiO_2 and only Cr on the mesh under visible light illumination.

mesh based photocatalytic nanomaterials are efficient for removal of pollutants by both physical (filtration) and chemical (photocatalysis) processes. Liao *et al.* reported that a Ti/TiO_2 mesh photoelectrode is an excellent system for photocatalytic degradation of methyl orange in an aqueous solution.[59] Yong *et al.* reported that a heterostructure (CuO–ZnO) embedded on a stainless steel mesh exhibited excellent photocatalytic activity for a non-biodegradable azo dye.[60] In comparison with earlier reports, we expect that our approach will not only be cost effective but will also offer decontamination of drinking water in a promising way for real world application (Scheme 1).

4. Conclusion

We have successfully synthesized (Cu)PP–TiO_2 nanohybrids for the reduction of toxic Cr(VI) metal ions under visible light illumination. The (Cu)PP–TiO_2 nanohybrids exhibit an efficient photocatalytic activity and recyclability compared to PP–TiO_2. In addition, the presence of dissolved Cr^{3+} and Fe^{3+} metal ions in drinking water significantly reduces the photocatalytic activity of PP–TiO_2, while (Cu)PP–TiO_2, with enhanced photostability, shows an insignificant decrease in photocatalytic activity. The tuning of photocatalytic activity of the nanohybrids in the presence of dissolved metal ions can be correlated with ultrafast dynamical events, observed from a time-resolved fluorescence study. We have also developed a prototype for real world application. In this context, the (Cu)PP–TiO_2 nanohybrid fabricated on a stainless-steel mesh is shown to be efficient for the reduction of toxic Cr(VI) metal. The photocatalyst, *i.e.* (Cu)PP–TiO_2, functions as a chemical cleaning agent to detoxify the toxic Cr(VI) to non-toxic Cr(III), and the host mesh acts as a physical filter to remove suspended particulates including the non-toxic/insoluble photo-reduced product. This dual cleaning action of the prototype efficiently separates the product, which is essentially suspended particulates from water, and blocks the possibility of re-oxidation of Cr(III) to Cr(VI) under an ambient natural/physiological environment. This novel prototype may

act as a promising device for practical water purification application to combat aqua-chromium hazards.

Conflicts of interest

There are no conflicts to declare.

Acknowledgements

P. K. thanks the Council of Scientific and Industrial Research (CSIR, India) for fellowship. T. K. M. thanks DST-INSPIRE for fellowship. We are thankful to DBT (India), DST (India) for financial grants BT/PR11534/NNT/28/766/2014, DST-TM-SERI-FR-117 and EMR/2016/004698. P. L. thanks the NTH-School 'Contacts in Nanosystem: Interaction, Control and Quantum Dynamics', the Braunschweig International Graduate School of Metrology, and DFG-RTG 1953/1, Metrology for Complex Nanosystems.

References

1 M. Zhang, C. Shao, Z. Guo, Z. Zhang, J. Mu, T. Cao and Y. Liu, *ACS Appl. Mater. Interfaces*, 2011, **3**, 369–377.
2 M.-Y. Chang, Y.-H. Hsieh, T.-C. Cheng, K.-S. Yao, M.-C. Wei and C.-Y. Chang, *Thin Solid Films*, 2009, **517**, 3888–3891.
3 S. K. Cushing, F. Meng, J. Zhang, B. Ding, C. K. Chen, C.-J. Chen, R.-S. Liu, A. D. Bristow, J. Bright, P. Zheng and N. Wu, *ACS Catal.*, 2017, **7**, 1742–1748.
4 L. M. Peter, *J. Phys. Chem. Lett.*, 2011, **2**, 1861–1867.
5 J. W. Dobrucki, *J. Photochem. Photobiol., B*, 2001, **65**, 136–144.
6 J. N. Demas, D. Diemente and E. W. Harris, *J. Am. Chem. Soc.*, 1973, **95**, 6864–6865.
7 S. Sarkar, A. Makhal, T. Bora, K. Lakhsman, A. Singha, J. Dutta and S. K. Pal, *ACS Appl. Mater. Interfaces*, 2012, **4**, 7027–7035.
8 S. Afzal, W. A. Daoud and S. J. Langford, *J. Mater. Chem.*, 2012, **22**, 4083–4088.
9 V. K. Gupta, I. Ali, T. A. Saleh, M. Siddiqui and S. Agarwal, *Environ. Sci. Pollut. Res.*, 2013, **20**, 1261–1268.
10 B. Sun, E. P. Reddy and P. G. Smirniotis, *Environ. Sci. Technol.*, 2005, **39**, 6251–6259.
11 D. R. Mount and J. R. Hockett, *Water Res.*, 2000, **34**, 1379–1385.
12 X. Zhou, T. Korenaga, T. Takahashi, T. Moriwake and S. Shinoda, *Water Res.*, 1993, **27**, 1049–1054.
13 M. D. Cohen, B. Kargacin, C. B. Klein and M. Costa, *Crit. Rev. Toxicol.*, 1993, **23**, 255–281.
14 A. H. Smith and C. M. Steinmaus, *Annu. Rev. Public Health*, 2009, **30**, 107–122.
15 D. Bagchi, S. J. Stohs, B. W. Downs, M. Bagchi and H. G. Preuss, *Toxicology*, 2002, **180**, 5–22.
16 S. A. Katz and H. Salem, *J. Appl. Toxicol.*, 1993, **13**, 217–224.
17 G. M. Keegan, I. D. Learmonth and C. Case, *Crit. Rev. Toxicol.*, 2008, **38**, 645–674.
18 A. M. Alansi, M. Al-qunaibit, I. O. Alade, T. F. Qahtan and T. A. Saleh, *J. Mol. Liq.*, 2018, DOI: 10.1016/j.molliq.2018.01.034.
19 T. A. Saleh, S. Agarwal and V. K. Gupta, *Appl. Catal., B*, 2011, **106**, 46–53.
20 V. K. Gupta, I. Ali, T. A. Saleh, A. Nayak and S. Agarwal, *RSC Adv.*, 2012, **2**, 6380–6388.
21 B. Sun, E. P. Reddy and P. G. Smirniotis, *Appl. Catal., B*, 2005, **57**, 139–149.
22 E. P. Reddy, B. Sun and P. G. Smirniotis, *J. Phys. Chem. B*, 2004, **108**, 17198–17205.
23 M. N. Chong, B. Jin, C. W. K. Chow and C. Saint, *Water Res.*, 2010, **44**, 2997–3027.
24 K. Kabra, R. Chaudhary and R. L. Sawhney, *Ind. Eng. Chem. Res.*, 2004, **43**, 7683–7696.
25 J. Wu, J. Wang, Y. Du, H. Li, Y. Yang and X. Jia, *Appl. Catal., B*, 2015, **174–175**, 435–444.
26 T. A. Saleh, *Advanced Nanomaterials for Water Engineering, Treatment, and Hydraulics*, IGI Global, 2017, ISBN13: 9781522521365.
27 T. A. Saleh and V. K. Gupta, *Nanomaterial and Polymer Membranes: Synthesis, Characterization, and Applications*, Elsevier, 2016, ISBN13: 9780128047033.
28 M. Celebi, M. Yurderi, A. Bulut, M. Kaya and M. Zahmakiran, *Appl. Catal., B*, 2016, **180**, 53–64.
29 M. Celebi, K. Karakas, I. E. Ertas, M. Kaya and M. Zahmakiran, *ChemistrySelect*, 2017, **2**, 8312–8319.
30 D. Liu, M. W. Zhang, W. J. Xie, L. Sun, Y. Chen and W. W. Lei, *Catal. Sci. Technol.*, 2016, **6**, 8309–8313.
31 Y. Zhao, D. Zhao, C. Chen and X. Wang, *J. Colloid Interface Sci.*, 2013, **405**, 211–217.
32 P. Kush, K. Deori, A. Kumar and S. Deka, *J. Mater. Chem. A*, 2015, **3**, 8098–8106.
33 D. K. Padhi and K. Parida, *J. Mater. Chem. A*, 2014, **2**, 10300–10312.
34 N. Wang, L. Zhu, K. Deng, Y. She, Y. Yu and H. Tang, *Appl. Catal., B*, 2010, **95**, 400–407.
35 A. D. Apte, V. Tare and P. Bose, *J. Hazard. Mater.*, 2006, **128**, 164–174.
36 Z.-Q. Li, Y.-P. Que, L.-E. Mo, W.-C. Chen, Y. Ding, Y.-M. Ma, L. Jiang, L.-H. Hu and S.-Y. Dai, *ACS Appl. Mater. Interfaces*, 2015, **7**, 10928–10934.
37 B. Liu, L.-M. Liu, X.-F. Lang, H.-Y. Wang, X. W. Lou and E. S. Aydil, *Energy Environ. Sci.*, 2014, **7**, 2592–2597.
38 P. Kar, S. Sardar, E. Alarousu, J. Sun, Z. S. Seddigi, S. A. Ahmed, E. Y. Danish, O. F. Mohammed and S. K. Pal, *Chem.–Eur. J.*, 2014, **20**, 10475–10483.
39 Y. C. Zhang, L. Yao, G. Zhang, D. D. Dionysiou, J. Li and X. Du, *Appl. Catal., B*, 2014, **144**, 730–738.
40 B. Liu and H. C. Zeng, *Chem. Mater.*, 2008, **20**, 2711–2718.
41 G. B. Deacon and R. J. Phillips, *Coord. Chem. Rev.*, 1980, **33**, 227–250.
42 A. Marcelli, I. Jelovica Badovinac, N. Orlic, P. R. Salvi and C. Gellini, *Photochem. Photobiol. Sci.*, 2013, **12**, 348–355.
43 S. Sardar, P. Kar and S. K. Pal, *Journal of Materials NanoScience*, 2014, **1**, 12–30.
44 S. Verma, A. Ghosh, A. Das and H. N. Ghosh, *J. Phys. Chem. B*, 2010, **114**, 8327–8334.
45 N. C. Maiti, S. Mazumdar and N. Periasamy, *J. Phys. Chem. B*, 1998, **102**, 1528–1538.

46 G. Granados-Oliveros, E. A. Páez-Mozo, F. M. Ortega, C. Ferronato and J.-M. Chovelon, *Appl. Catal., B*, 2009, **89**, 448–454.
47 P. Kar, T. K. Maji, J. Patwari and S. K. Pal, *Mater. Chem. Phys.*, 2017, **200**, 70–77.
48 Q. Wu, J. Zhao, G. Qin, C. Wang, X. Tong and S. Xue, *Appl. Catal., B*, 2013, **142–143**, 142–148.
49 X. F. Lei, X. X. Xue and H. Yang, *Appl. Surf. Sci.*, 2014, **321**, 396–403.
50 J. Yang, J. Dai and J. Li, *Environ. Sci. Pollut. Res.*, 2013, **20**, 2435–2447.
51 X. Liu, L. Pan, T. Lv, Z. Sun and C. Sun, *J. Mol. Catal. A: Chem.*, 2012, **363–364**, 417–422.
52 X. Liu, L. Pan, T. Lv, G. Zhu, Z. Sun and C. Sun, *ChemComm*, 2011, **47**, 11984–11986.
53 P. Kar, T. K. Maji, R. Nandi, P. Lemmens and S. K. Pal, *Nano-Micro Lett.*, 2016, **9**, 18.
54 P. Kar, S. Sardar, S. Ghosh, M. R. Parida, B. Liu, O. F. Mohammed, P. Lemmens and S. K. Pal, *J. Mater. Chem. C*, 2015, **3**, 8200–8211.
55 X. Zhao, Y. Wang, W. Feng, H. Lei and J. Li, *RSC Adv.*, 2017, **7**, 52738–52746.
56 Y. Zhang, Z. Chen, S. Liu and Y.-J. Xu, *Appl. Catal., B*, 2013, **140–141**, 598–607.
57 L. Shao, J. Li, X. Liang, T. Xie, S. Meng, D. Jiang and M. Chen, *RSC Adv.*, 2016, **6**, 18227–18234.
58 X. Wang, S. O. Pehkonen and A. K. Ray, *Ind. Eng. Chem. Res.*, 2004, **43**, 1665–1672.
59 J. Liao, S. Lin, L. Zhang, N. Pan, X. Cao and J. Li, *ACS Appl. Mater. Interfaces*, 2012, **4**, 171–177.
60 S. Jung and K. Yong, *ChemComm*, 2011, **47**, 2643–2645.

